Manuscript Number: B0.1-PE-0002

RADAR MEASUREMENTS OF THE REENTRY OF THE ARIANE 504 EPC

R. Reynolds [1], J. Jost [2], G. Rubin [1], J. Vila [3]

[1] *Center for Radar Physics, System Planning Corporation, Arlington, VA, 22209 USA*; [2] *Aeroflex/Lintek Radar Systems, Powell, OH 43065 USA*; [3] *CNES DLA, Rond Point de l'Espace, 91023 Evry, FRANCE*

ABSTRACT

A new VHF radar system has been integrated onto a KC-135 aircraft to provide a mobile platform for observing reentry of the Ariane 5 Main Cryogenic Stage (EPC). This system was flown successfully in performing measurements of reentry of the EPC from the Ariane 504 launch occurring on December 10, 1999. The primary requirement was to obtain the altitude of breakup of the EPC. Secondary requirements were to characterize the breakup, including searching for debris that might survive reentry, and to provide data on the reentry trajectory. Breakup was observed to begin somewhat above 70 km altitude, with evidence that fragmentation of the main structure continued over an 8 second interval, making the process somewhat higher in altitude than observed for Ariane 503. Multipath interference was observed in the long pulse transmission mode, and these data were used to obtain a direct measurement of EPC altitude as a function of time.

This paper discusses the underlying concepts that contributed to planning the data acquisition and presents results of those measurements. This paper also discusses the data and data processing, leading up to a discussion of the results and lessons learned during the data reduction and analysis process.

INTRODUCTION

Ariane 5 Background

Ariane 5 is the European heavy launcher that, after two successive qualifications flights, entered commercial life on December 10, 1999, with flight 504. The design of Ariane 5 is structured around two solid boosters, the Etage Principal Cryotechnique (EPC, the main cryogenic stage), and a storable propellant upper stage as shown in Figure 1.

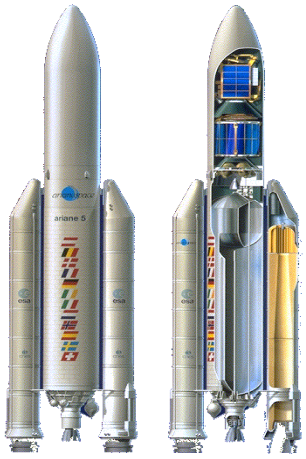

Figure 1. Ariane 5 launcher

Ariane 5 launch trajectories are planned so that the EPC is left on a reentering orbit after burnout. This is done to avoid any risk associated with an uncontrolled reentry over inhabited areas. Although the EPC is mainly composed of large structures of light alloy that should melt during reentry, several massive parts may survive reentry. Extensive studies during Ariane 5 development have demonstrated that some pieces, such as the engine, turbopumps, and titanium tanks, might survive reentry and represent an unacceptable risk of injuring people should they fall on inhabited territory. For each Ariane 5 mission, the launch trajectory is thus constrained so that the debris falls into uninhabited zones in the Pacific Ocean. The EPC undergoes controlled reentry (at 120,000 m) with typical speeds of 7000 to 7600 m/s and a flight path angle of –2° to –4°.

After burnout and separation from the upper stage, the EPC is passivated by pyrotechnically opening depressurization valves. The aim of this passivation process is to remove the risk of highly energetic explosion of the stage during reentry which could disperse debris over a large area. The depressurization valve nozzle of the hydrogen tank causes the outgassing to create a torque during passivation. This torque induces a tumbling motion of the stage along its reentry trajectory with a typical rotation speed of 60°/s. This tumbling motion eliminates the risk of skipping or bounce effect at EPC reentry which could cause the EPC to reenter over land. At reentry, aerodynamic pressure and thermodynamic fluxes induce a smooth breakup of the stage that was calculated to occur between 60 and 85 km altitude.

Reentry Observations Background

The goal of the System Planning Corporation Ariane-5 EPC Reentry Characterization Program is to design, develop, test, and qualify an airborne radar system to perform a series of reentry observations of the EPC, the main cryogenic stage of the Ariane 5 launch vehicle. To accomplish this goal, a long-range Multiband Airborne Radar System (MARS) has been developed and installed on a United States Air Force KC-135 aircraft shown in Figure 2.

The project is funded and managed through the Direction des Lanceurs (Launch Vehicle Directorate) of the Centre National d'Etudes Spatiales (CNES, the French Space Agency). System Planning Corporation is responsible for the radar and acquiring and analyzing the data. Airframe integration and flight support is provided by the US Army Big Crow Program Office (BCPO). Reentry observations of the EPC from the Ariane 504 mission were used to qualify the system and technique.

Fig. 2. Airborne Radar Platform (BCPO KC-135) with VHF Antennas Mounted on the Cargo Bay Door

The primary instrument for MARS is a long-wavelength (49.92 MHz) VHF radar, which has sufficient sensitivity to acquire and track a reentering EPC at long range (>500 km) and to provide signature information on the reentry, breakup, and disintegration processes. A second independent instrument is a high frequency radar used for detecting hardbody returns and further characterizing reentry signatures. The radar system is integrated into a KC-135 aircraft, facilitating operations with minimal geographic constraint. The long-range requirement for MARS was established so that the inherent dispersions in the trajectory of the reentering EPC could be covered from a single observation point. A mission planning system was developed so that the only input data required from the Ariane program were the predicted EPC nominal and variance trajectories based on pre-launch models, and the nominal EPC trajectory based on the last good measured state vector at EPC main engine cutoff. This planning system was used for pre-flight planning, designing the test flights for system validation, and for directing flight operations on the day of launch. Additional information on the hardware and support system will be presented in a paper in preparation (Reynolds et al., 2000b).

DISCUSSION

A discussion of the operational approach, day of mission activities, and an in-depth discussion of all aspects of the data is beyond the scope of this brief paper. This information can be found in the Final Report for this mission (Reynolds et al., 2000a). In this paper the issues of multipath effects, range-azimuth coupling, and reentry ionization processes are briefly discussed to better understand the approach for the mission and the context for the data.

Overview of VHF Data

The VHF data came from two interlaced waveforms – one having a long pulse with low pulse repetition frequency (PRF) and the second having a short pulse at high PRF. The use of alternating dissimilar waveforms to maximize both unambiguous range and Doppler provided a unique data reduction challenge. In order to make proper use of the data, it was necessary to apply different processing methods to the high-PRF (Doppler unambiguous) and low-PRF (range unambiguous) data. Once a time interval was selected for analysis of return data, it was necessary to locate data from the desired waveform within the data file. This was done in a two-step process. First, the data was searched for peaks representing the transmit pulse. These peaks were significantly higher than those from any reflected energy, preventing possible misidentification of pulses. Once the locations of the transmit pulses were identified in the data file and indexed by byte address, the time (Δt) between successive indices could be used to determine the type of waveform. Changes in Δt would then reflect a transition from one waveform to the other. The byte addresses corresponding to the waveform transitions were finally recorded in two files, one representing the beginning of high-PRF pulses and the other representing the beginning of low-PRF pulses. These files were then used in data processing to jump to either high-PRF or low-PRF waveforms as desired.

In processing the VHF data, the aim was to maximize signal-to-noise ratio (SNR) and obtain information about range, altitude, and velocity. The low-PRF data was generally used for range processing, as the long time between pulses provided a large unambiguous range window. Similarly, the Doppler processing was generally performed on the high-PRF data set to take advantage of its large unambiguous Doppler window. The processing was not limited to these pairings, however, and examining the Doppler spectra contained in the low-PRF data revealed additional information. To increase SNR in the low-PRF data sets, an iterative process was developed to remove DC-bias from the I and Q channels. This routine used the noise immediately in front of the return signal as a reference.

In order to obtain range information, individual pulse returns were plotted in a Range-Time-Intensity plot. If desired, the data could first be run through a matched filtering (auto-correlation) routine, taking advantage of the known pulse parameters to emphasize peaks that might correspond to a reflected return. The mathematics associated with the matched filter process dictate that while the SNR of peaks of the same dimensions as the pulse may be increased, the range extent of the return is

altered. In order to decrease the uncertainty in the range measurements, matched filtering was primarily used for qualitative analysis only.

The data discussed in this paper were acquired primarily from the low PRF waveform, which had a pulse length of 133 μs and a PRF of 150 Hz. Figure 3 presents the range versus time data from this waveform. The narrow gaps in the data show where the high PRF waveform is being transmitted, and the wide gaps were times where pulse blanking was used to insert fiducial reference points into the data. The first evidence of returns occurs at 6096 seconds mission elapsed time (MET) at a range of 465 km. Data continues to be seen through minimum range, occurring at 6133 seconds MET and a range of 294 km, and then persists until 6150 seconds MET. Early in reentry, persistent high-altitude ionization features can be seen at ranges of 455, 425, and 395 km. The bright flash at minimum range is the specular reflection off of the ionization cloud that occurs when the radar beam is normal to the direction of flight (and therefore normal to the long axis of the ionization cloud).

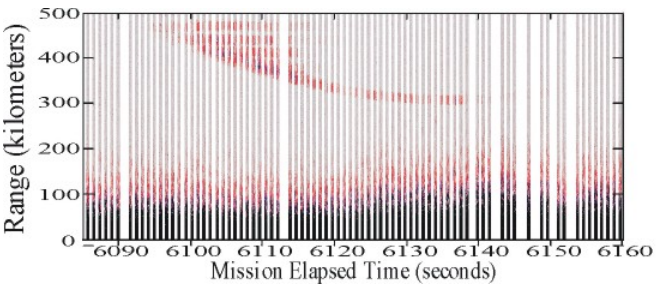

Fig. 3. Processed range versus time for Low-PRF data

Measuring EPC Altitude from Multipath Returns

Multipath effects, which can have an impact on radar performance, have been studied extensively (see, for example, Chapter 6 in Blake 1986). However, the particular effect of interest here, determining target altitude using multipath effects has not been of great interest. In part this is because the problem is itself of only special interest, but also because the concept as developed here is specific to an airborne radar reflecting off the ocean surface. Consequently, the results developed here are not found readily in the literature.

The geometry for the multipath analysis is presented in Figure 4. The radar is located at P and the EPC at T. The altitude of the radar, h_P, is known (8.5 km for these data). Given that the angle of incidence onto the ocean surface equals the angle of reflection off of the ocean surface, denoted θ, there is enough information to solve 2 types of problems. First, given the latitude, longitude, and altitude of the EPC and the radar, calculate R, R_1, and R_2; this form is used to predict multipath effects. Second, given data, which is effectively R and R_1+R_2, determine the altitude of the EPC (h_T); this form is used to interpret the data. The low PRF waveform created an interference pattern between the direct path (path length = 2R), the two single bounce paths that consisted of a direct segment and one bouncing off the ocean surface (path length = $R+R_1+R_2$), and the double bounce return (path length = $2R_1+2R_2$).

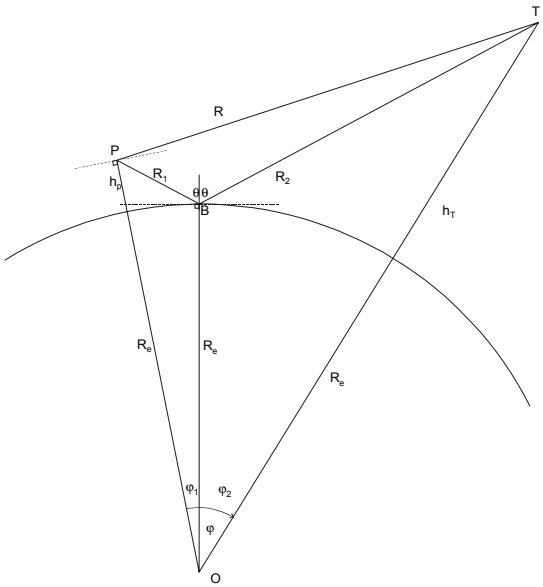

Fig. 4. Geometry for multipath analysis

Figure 5 clearly shows the time phased contribution from each of the three components in the return signal strength versus signal propagation time. This trace was generated by coherently adding 64 returns at minimum range. Defining slant range to a target to be one-half the signal travel time times the speed of light, the slant ranges for the direct, single bounce, and double bounce paths are R, $(R_1+R_2+R)/2$, and R_1+R_2 respectively. The differences in slant range between the direct and single- and double-bounce signals, $(R_1+R_2-R)/2 \equiv S_1$ and R_1+R_2-R respectively, are plotted in Figure 6 as a function of MET for a best fit trajectory model.

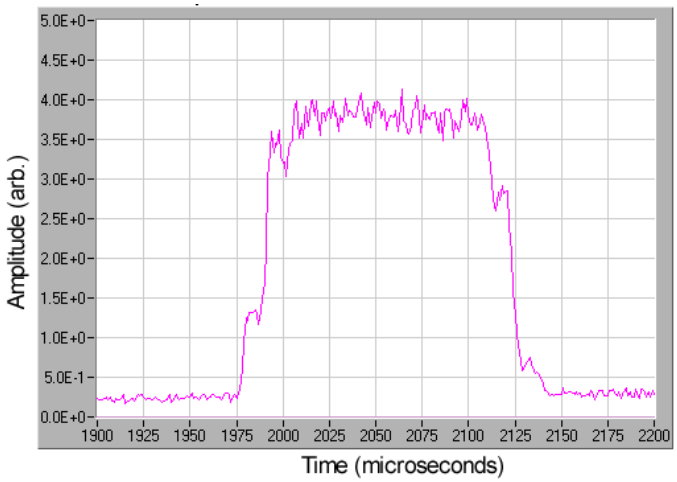

Fig. 5. Return signal strength vs. time at minimum range

Assuming a flat Earth yields analytic expressions that provide sensitivities of the measured quantities. In this approximation and assuming further that $R_1+R_2+R \approx 2R$ it can be shown that

$$RS_1 = h_p h_T . \quad (1)$$

Given that the altitude of the radar is constant, variation of this equation yields an expression for sensitivity of h_T to R and S_1.

$$\delta h_T = \frac{R}{h_p}\delta S_1 + \frac{S_1}{h_p}\delta R . \quad (2)$$

In general, R is a few 100's of kilometers whereas S_1, as seen in Figure 6, is on the order of a few kilometers. Consequently, the measured EPC altitude is in general much more sensitive to the measured difference in slant range of the direct and single bounce indirect returns than it is to the range itself. It is interesting to note that at times where extrema occur in the range or range difference curves Eq. 2 yields a simple measure of the time rate of change of altitude of the EPC.

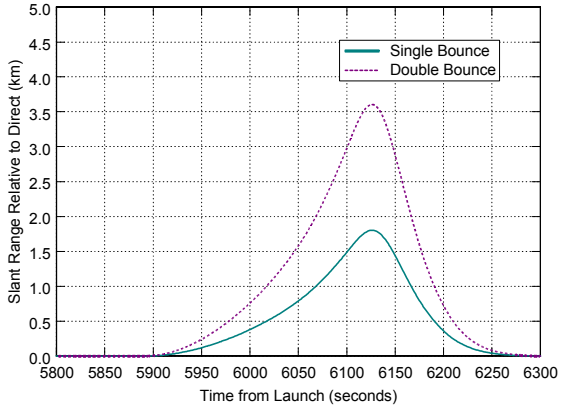

Fig. 6. Range difference between the direct return and the multipath returns

The above analysis ignores the effects of atmospheric refraction, which could be important because it will bias the altitude calculation. The effects of refraction will be two-fold: (1) to slow the speed of the signal propagation which causes the straight line rays shown in Figure 4 to curve and thereby (2) to increase the propagation distance. Since the aircraft was at an altitude of 8.5 km, refraction effects on the direct ray are less important than for the reflected ray, which propagates to sea level and back out. The effect on the difference in arrival times would be expected to be systematic, in the sense that it should add more delay to the reflected ray path than to the direct path. This will make the time separation between arrival times larger than the unrefracted model would expect. By making S_1 larger the calculated altitude of the EPC will be higher than it should be.

Using a standard tropical atmosphere model (McKinley, 1961) and an atmospheric index of refraction model that depends on neutral atmospheric density, water vapor content, and temperature (Wolfe and Zissis, 1985), a model was developed to correct for refraction effects. These corrections were found to vary from roughly 0.5 km at minimum range to 2 km at long range. These corrections are smaller than the expected uncertainty arising from time resolution in the data. One problem with refraction is that local atmospheric conditions can experience significant temporal and spatial changes in the index of refraction relative to the mean atmosphere, so there will always be uncertainty in the magnitude of the refraction effect that cannot be measured.

Directional Determination Based on Range

The azimuth to the EPC, α, can be quite accurately determined from the azimuth to the minimum range point, α_{MIN}, the range, R, and minimum range, R_{MIN}, from the equation

$$R = R_{MIN}\sec(\alpha - \alpha_{MIN}). \quad (3)$$

The range is measured, and the azimuth at minimum range and a good estimate of minimum range is given from the two points provided by CNES after EPC burnout. The accuracy of this azimuth can be seen from Figure 7 where range versus azimuth plots are presented for the three pre-mission orbits provided by CNES and using Eq. 3. It can be seen in this figure that not only do the various trajectories overlap except near minimum range, but they also fit the secant function well. At long range the azimuth is independent of R_{MIN} and very sensitive to range, thereby determining azimuth accurately.

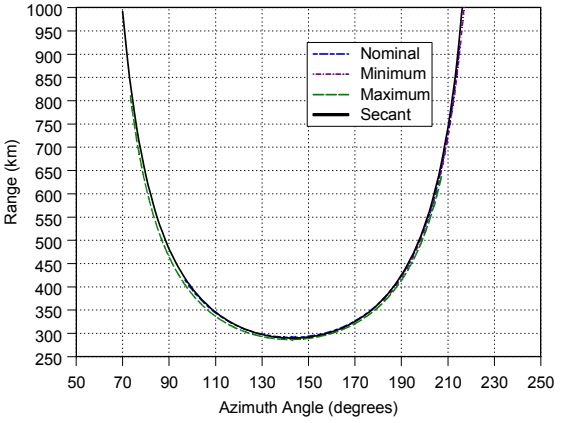

Fig. 7. Plot of range versus azimuth for three model orbits and the secant function

Fitting Range Data to Model Predictions

A plot of the raw measurement data, best fit model, and a constant velocity hyperbola (8.05 km/s) are shown in Figure 8. In general there is a good fit between the three before minimum range is attained, but past minimum range, where the altitudes are lower, the model shows a hyperbola-like behavior, but with lower characteristic velocity (the more open the hyperbola, the lower the velocity). At longest range, the data appears at longer range than predicted or, alternatively, at later time than it

should for the observed range. This anomaly in the data is explained by the latter interpretation. That is, that there is a time delay between creation of the ionization and detection at long range, during which the ionization cloud expands and increases its RCS. Modeling the ionization cloud as an expanding cylinder and observing that the maximum range at which no delay time is encountered to be 350 km, an effective diffusion velocity of 6 m/s is required to shift that data to a creation time consistent with the models. The implied diffusion velocity for this delay is consistent with diffusion coefficients for this altitude range of 6 m^2/s [6].

MEASUREMENT RESULTS

Measurement of EPC Altitude

A plot of the measured altitudes as a function of time is presented in Figure 9. The first six data points were taken from the low-PRF data where there was the least uncertainty in selecting the range for the return amplitude jumps. The last two points were taken from the high-PRF data near minimum range, when the multipath returns emerged. The "error" bars show the change in altitude induced by a 1 μs change in the direct return step. The "×" associated with each altitude point shows the altitude corrected for refraction. The figure also shows the linear least squares fit to the corrected altitude. The χ^2 value of these data points for their fit to the best fit model is 0.997.

Determination of Breakup Time

The Range-Time-Intensity data show a time-dependent behavior that is associated with a tumbling motion of the EPC. These data have been scaled in Figure 10 to emphasize this periodicity. The peaks are relatively constant and separated in time by roughly 2.7 seconds, implying a relatively simple tumble motion at a rate of about 67 °/s, with peaks in the amplitude occurring every half revolution where the EPC is presenting its largest area to the atmosphere. Peaks from the tumble are seen to be the source of the persistent apparent striations that are seen early in the reentry.

The amplitudes follow a pattern until after the peak at 6123 seconds MET (Block 87). The next peak and following peaks are significantly different, and are attributed to breakup being initiated when the EPC was broadside to the atmosphere at 6123 seconds. The flash at 6126 seconds MET (Block 102) is from intense ionization associated with the EPC still in the early stages of breaking up as it once again comes broadside to the atmosphere. The only significant flash after breakup occurs at 6133 seconds (Block 113), when the EPC debris cloud is at minimum range and there is a specular reflection off of the ionization cloud.

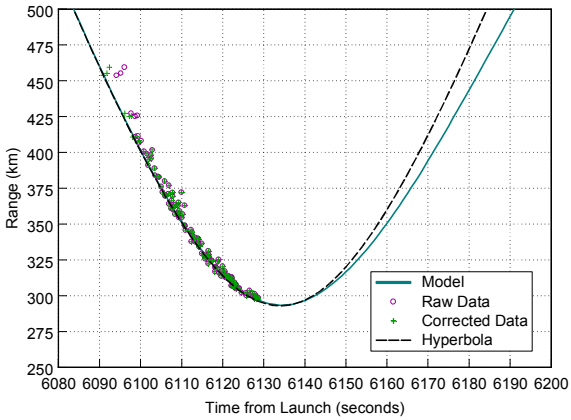

Fig. 8. Range versus time for Best-Fit Model, a constant velocity hyperbola, raw data, and data corrected for ionization cloud growth

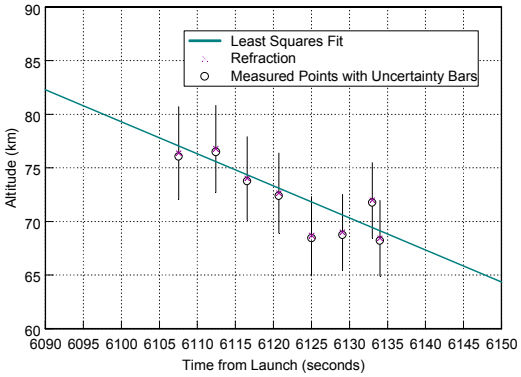

Fig. 9. Altitude measurements using multipath analysis

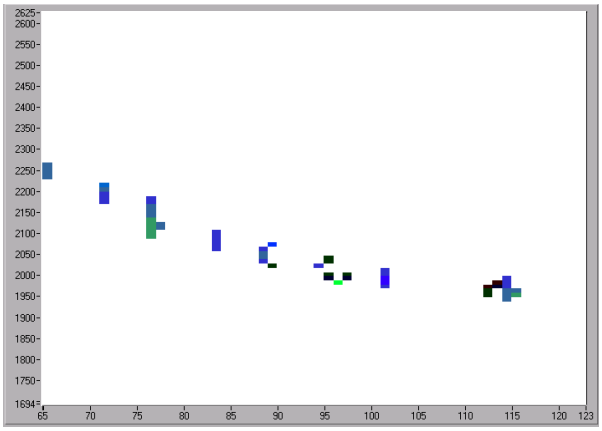

Fig. 10. Range (ns) versus time (pulse block) showing return signal strength oscillation

Understanding the Reentry Processes: Comparison of the Data with the Model

Much of the understanding of the range versus time relationship shown in Figure 3 is expedited by comparing the data to expected results from modeling the reentry. To make this comparison, a best fit model for range versus time was defined, to build up a consistency between information the data is carrying and what the theory would predict. This comparison can be made with some confidence because at altitudes above 70 km, with the steep reentry of the EPC, the aerodynamic effects would appear to be minimal and therefore uncertainties in the EPC drag and atmosphere characteristics are not important. This is illustrated in Figure 11 in a plot of longitude of ascending node (LAN) of the reentry trajectory versus time. In this plot, if the trajectory is following a plane in inertial space, the LAN will move westward at roughly 15 °/h (parallel to the inertial rate

line), while if it is co-moving with the atmosphere it remains at a fixed value. It can be seen in this figure that to 6180 seconds MET (corresponding to an altitude of 51 km) the plane stays nearly inertial. Below 51 km the trajectory transitions to co-moving with the atmosphere, becoming co-moving slightly after 6270 seconds MET (corresponding to an altitude of 20 km). What is important from this figure is to conclude that the reentry kinematics to altitudes above 60 km, which includes the breakup, aerodynamic effects may be treated as perturbations to the inertial kinematics.

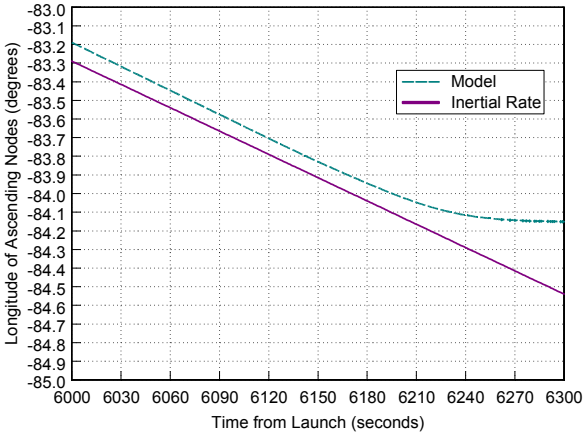

Fig. 11. Longitude of ascending node of nominal reentry trajectory versus time

Characterization of the Breakup Process

The debris cloud expansion rate was calculated from the debris cloud cross-range extent measured at minimum range (6133 seconds MET). The measured cross-range extent at this time was 977 meters. Because there had been 11 seconds since the breakup time of 6122 seconds MET, this leads to expansion velocities somewhat less than 100 m/s. Residual LOX/LH_2 propellants in the EPC were vented, so only aerodynamic effects contributed to the breakup velocity and these perturbations were small as expected. The fact that the event was not highly energetic is also to be inferred from the fact that there was no strong flash of ionization that would be expected to be associated with a large release of energy at breakup.

In measurements of reentry of the STS-33 External Tank the breakup process more closely resembled an explosion rather than the breakup predicted from reentry models. The identification of the event as explosive occurred because the number of fragments observed and the velocity spreading were found to be consistent with the numerous on-orbit explosions that have contributed so much to the orbital debris population. The source of energy for this explosion was the same as that for many on-orbit explosions - the ignition of residual propellant. On the External Tank there was a residual of LOX/LH_2 in a sealed volume, and as the tank began to fail these components would have warmed, vaporized, mixed and ignited.

Debris Surviving to Lower Altitudes

It was not possible with the data as processed to characterize individual debris fragments surviving after the breakup process. However, there are low PRF returns still evident in the data at 6150 seconds MET, so there is material that has survived to an altitude of 60 km. These objects have undergone significant aerobraking, having velocities on the order of 7 km/s, so some of the debris may have survived to ground impact.

The RCS value for the ionization at 60 km altitude were 30-40 dBsm. A first-order estimate of the corresponding "size" can be made by assuming that the scattering was from a rapidly quenching ionization sphere for a single debris component (or a composite return from several debris components). At a frequency of 49.92 MHz a 30 dBsm scatterer will be in the Mie or pseudo-optical region of the Rayleigh curve. For a single source this leads to a sphere of radius ~35 meters, which we believe indicates several objects were still generating ionization returns below 60 km. Clearly, there is significant long-lived debris that needs to be investigated carefully on future missions.

Flash Feature at 6108 seconds MET

The flare event seen at 6108 seconds MET, which corresponds to an altitude of ~78 km, indicates a burst of ionization occurred at that time. The event does not appear to be related to major structural change, as there is still well defined tumble motion by the EPC after the event. One explanation of the event is that the cryogenics remaining within the vented tanks became heated and flashed off as a vapor. The release of a gas cloud moving at some 8 km/s relative to the atmosphere would have produced a great deal of ionization as the gas collisionally interacted with the surrounding atmosphere.

This release of gas might also account for an apparent discrepancy between the tumble rate and the change in range seen prior to the event. The ranges for the banding in the persistent high altitude features do not appear to be consistent with the 67 °/s observed after the flare event, but instead would require a lower tumble rate at high altitude. The gas release associated with the flare could then be seen as occurring in such a way that it caused the EPC to increase its tumble rate

Persistent Features at High Altitude

One of the interesting features in the data is the persistent ionization returns associated with passage of the EPC through the atmosphere at altitudes above 85 km. This is occurring in a region where recombination or reattachment rates are low because of the low atmospheric density, but may also reflect wavelike disturbances that propagate through the naturally occurring plasma at these altitudes. The fact that these features drop in intensity at about the same time is probably an indication of the atmospheric density distribution with altitude in that region. Figure 12 presents a plot of SNR as a function of time for this persistent ionization feature. The initial growth in SNR that is seen in this figure is consistent with the growth

times required to correct the range data as derived in the discussion on ionization cloud growth. The gap at roughly 6112 seconds MET shows pulse-blanking.

The conclusions are summarized in Table 1. The objective reflects the priority of attaining that objective as determined at the beginning of the project.

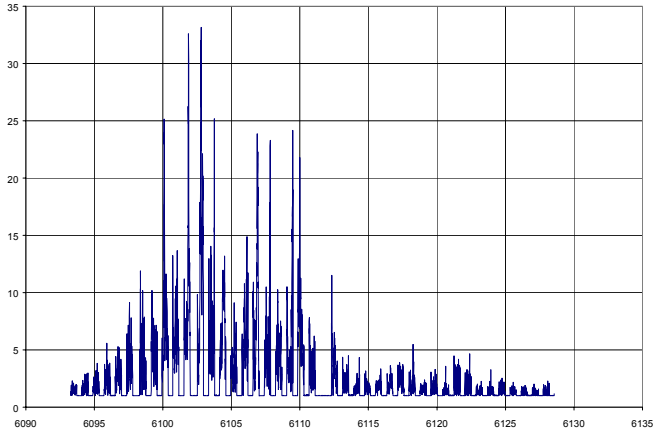

Fig. 12. SNR vs. Time of persistent ionization feature at 450 km slant range

Table 1. Conclusions from VHF Radar Data Analysis

Characteristic	*Observations Results*	*Objective*
Breakup Altitude	72-70 km (process is continuous)	Primary
Mode of Rupture	Benign aerodynamic breakup (non-explosive)	Secondary
Debris Cloud Expansion Rate	<100 m/s	
Surviving Pieces	Ionization observed to below 60 km altitude	
Entry Velocity	8.05 km/s	Additional
Entry Tumble Rate	67^{o} per second; consistent with bicycle mode	

REFERENCES

Blake, L. V., Radar Range-Performance Analysis, Artech House Inc., Norwood, MA, 1986.

McKinley, D.W.R., Meteor Science and Engineering, McGraw-Hill, NewYork, 1961

Reynolds, R., J. Jost, and G. Rubin, Final Report for the Ariane 5 EPC Reentry Characterization Program: System Validation and Observations of Mission V504, System Planning Corp. Technical Report, 2000a.

Reynolds, R., J. Jost, G. Rubin, M. Schuetze, J. Zimmerman, J. Vila, *A Multifrequency Airborne Radar System for Observing Space System Reentry*, 51st International Astronautical Congress, Paper IAA-00-IAA.6.5.09, 2000b.

Wolfe, W. and G. Zissis, Infrared Handbook, Revised Edition, Office of Naval Research, Department of the Navy, Arlington, VA, 1985